Optics Letters

Non-destructive characterization of rare-earth-doped optical fiber preforms

Marilena Vivona,* Jaesun Kim,† and Michalis N. Zervas

Optoelectronics Research Centre (ORC), University of Southampton B53, SO17 1BJ Southampton, UK
**Corresponding author: m.vivona@soton.ac.uk*

Received 5 June 2018; revised 26 June 2018; accepted 26 June 2018; posted 27 June 2018 (Doc. ID 334155); published 5 October 2018

We present a non-destructive optical technique for rare-earth-doped optical fiber preform inspection, which combines luminescence spectroscopy measurements, analyzed through an optical tomography technique, and ray-deflection measurements for calculating the refractive-index profile (RIP) of the sample. We demonstrate the technique on an optical fiber preform sample with a Yb^{3+}-doped aluminosilicate core. The spatial distribution of the photoluminescence signals originating from Yb^{3+}-single ions and from Yb^{3+}-Yb^{3+} cluster sites were obtained inside the core. By modifying the characterization system, we were able to concurrently evaluate the RIP of the core and, thus, establish with good accuracy the dopant distribution within the core region. This technique will be useful for quality evaluation and optimization of optical fiber preforms.

OCIS codes: (060.2310) Fiber optics; (260.3800) Luminescence; (290.3030) Index measurements.

https://doi.org/10.1364/OL.43.004907

Rare-earth (RE)-doped optical fibers are among the key enabling technologies allowing the development of efficient amplifiers and high-power fiber lasers, which have revolutionized entire sectors, such as optical communications [1] and material processing [2]. However, new developments and progress in the field set increasingly stringent requirements on fiber technology. In particular, for RE-doped optical fibers, accurate control and characterization of the refractive-index profile (RIP) and the active dopant profile (ADP) are crucial for improving further the laser efficiency and overall performance. In certain circumstances, such as the case of heavily Yb^{3+}-doped high-power fiber lasers, clustering of Yb^{3+}-ions should be monitored, as it can have a severely limiting impact on the overall performance [3]. Although various techniques have been applied for accurate characterization of the RIP in fibers [4] and preforms [5–7], much less work has been done for ADP characterization. Even more important, so far, the discussed ADP characterization techniques are destructive [8,9], which severely limits their usefulness. The non-destructive acquisition of microscopic information regarding RE-distribution in optical preforms is important to optical fiber manufacturers, as it can provide useful information along the entire preform length. Such information can be used to identify best-suited preform parts and increase fiber yield and quality. In addition, newly emerging novel optical fibers with complex dopant distributions within the core area, such as confined dopants [10] or doped rings [11], will benefit from accurate non-destructive characterization of the RIP and ADP within the core at the preform stage.

In this context, we have considered the application of three-dimensional (3D) image representation techniques as a starting point for visualizing the internal microstructure of the optical preform and, in particular, the Yb^{3+}-ion and Yb^{3+}-Yb^{3+} cluster distribution. The imaging technology based on the emission computerized tomography (e-CT) is particularly powerful in producing slice images of 3D objects. e-CT is a well-established technique in domains, such as plasma diagnostics [12] or combustion analysis [13], while it is still emerging in optical material science applications [14]. The analytic procedure is based on the *projection-slice theorem*, which correlates function projections to the function itself [15]. For the case of a two-dimensional (2D) function f, this theorem establishes that the function projection (one-dimensional) on a certain direction corresponds to a preliminary Fourier transform of the 2D-function f subsequently sliced through its origin parallel to the direction of the considered projection. Mathematically, from the analysis of the integrated line-of-sight projection data through the calculation of an inverse Radon transform for each detected image pattern, it is possible to rebuild a whole true image of the object. This procedure reduces to the application of the Abel inverse transformation when the sample is characterized by a high degree of rotational symmetry [16], as the dopant radial distribution in optical fiber preforms is supposed to be to first approximation in most cases. One typical concern in the ADP reconstruction problem is the difficulty in establishing accurately the core center and edge positions of the investigated sample. In our case, the combined study of the optical core RIP using the same detection system allows us to overcome two difficulties: the core edge location and the evaluation of the degree-of-symmetry of the dopant distribution,

which are important parameters for a reliable application of the e-CT method. In addition, the combined knowledge of core RIP and ADP enables the accurate evaluation of the guiding and amplification fiber characteristics.

In this Letter, we present the application of the e-CT technique to the characterization of the emission signal of a Yb^{3+}-doped preform, suitable for high-power laser devices. Moreover, we combined it with a refractive-index analysis based on ray-deflection measurement technique [5]. Such a measurement technique provides the Yb^{3+} emission distribution within the preform core with respect to the refractive-index distribution. In addition, by adjusting for the chromatic focal length variation of the imaging system, the method is able to detect signals in different spectral regions. By the detecting the visible (VIS) luminescence, we can map the distribution of Yb^{3+}-Yb^{3+} clusters, the effect of which can be very important and detrimental in the performance of heavily doped samples [3].

To demonstrate the technique, an optical fiber preform, manufactured by modified chemical vapor deposition (MCVD) process, with a four-layer structure. Specifically, the preform optical core is made of aluminosilicate glass with a nominal diameter of about 1 mm and Yb^{3+}-ion doping obtained by the solution doping technique. The overall Yb^{3+}-emission spectrum in the near-infrared (NIR) region was monitored by an optical spectrum analyzer (not shown here).

The combined ADP and RIP preform characterization experimental setup is shown in Fig. 1. For the photoluminescence (PL) detection and ADP characterization, two fiberized pump laser sources at 976 nm were collimated by aspheric lenses and used to illuminate the optical preform from opposite sides, in order to achieve uniform excitation of the doped core. When the core is illuminated from one side only, a pronounced slope is present in the PL profile detected by the charge-coupled device (CCD), due to the pump absorption. Instead, with the two-sided illumination, the PL-projected profile becomes symmetric, and is used as a measure of uniform excitation. The PL emitted by the sample was collected at 90° with respect to the excitation arm. Specifically, the NIR emission of Yb^{3+}-ions and the VIS cooperative luminescence of Yb^{3+}-Yb^{3+} clusters were acquired by a CCD with 3296 × 2472 active pixels of 5.5 μm × 5.5 μm size and equipped with bandpass filters centered at 1050 ± 10 or 500 ± 40 nm, respectively. A MATLAB script was encoded to calculate the Yb^{3+} spontaneous emission distribution using an inverse Abel transform, implemented by a Fourier transform followed by a Hankel transform of the projected PL projection curves [15]. For the refractive-index characterization, parallel rays from a collimated white light (WL) source illuminate transversally the sample and their effective beam deflection, obtained by inserting a knife-edge spatial filter, were measured by the CCD and used to extract the RIP of the sample [5,6]. During the measurements, the preform was kept immersed in an index-matching oil.

First, we deal with the characterization of the RIP $\Delta n(r)$ of the optical preform. The steps applied for the $\Delta n(r)$ profile derivation are explained in Fig. 2. The CCD image of Fig. 2(a) shows the sample as illuminated by the WL source and half-blocked by the knife-edge filter. The insertion of the knife edge in the optical path of the transmitted rays acts as a spatial filter, allowing one to visualize and distinguish in a single black-and-white contrast line the ray-deflection as the rays traverse the refractive-index distribution in the sample. Specifically, the deflection angle $\varphi(x')$ was calculated considering the displacement $d(x')$ that expresses the vertical distance between the light ray emerging from the preform and the radial point of incidence (ideally corresponding to the filter edge) at the position x' on the CCD plane. Note that $x'y'$ is the plane of detection. This is converted to deflection angle $\varphi(x')$ by

$$\varphi(x') = \frac{d(x')\tan(\alpha)}{L}, \tag{1}$$

where α is the angle between the knife-edge filter and the y'-axis, and L is the distance between the center of the sample and the spatial filter position [5]. All parameters are shown in Fig. 2(b). It is worth mentioning that no dependence on the azimuthal position is considered, due to the assumed cylindrical symmetry of the sample. The deflection angle, derived for the experimental data by the use of Eq. (1), is shown in Fig. 2(c). In order to take into account the possible error in establishing the black-and-white contrast profile from the detected image [in Fig. 2(a)], we have considered the deflection angle curve resulting from the average of two symmetrized curves, obtained by

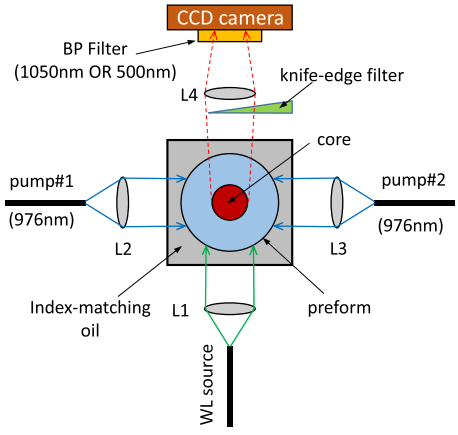

Fig. 1. Experimental setup for combined measurements of an ADP and RIP (RIP) in optical fiber preforms. (BP, bandpass; WL, white light; L, lens.)

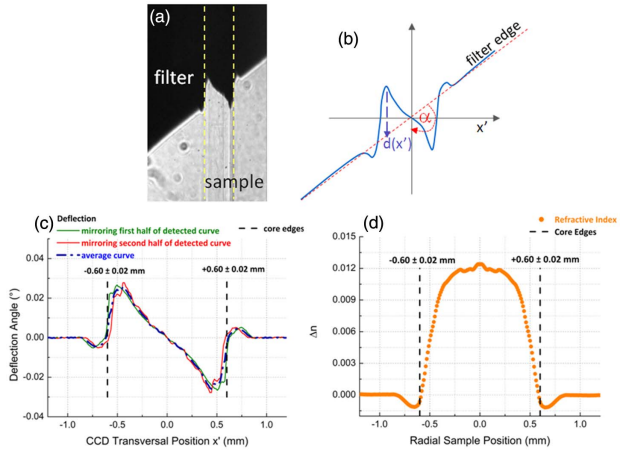

Fig. 2. (a) CCD image of the displacement highlighted by a knife-edge spatial filter, (b) parameters used for the deflection angle derivation, (c) the deflection angle function, and (d) the derived Δn core-cladding refractive-index difference.

mirroring the first or the second half of the experimental deflection curve, as detected by the CCD. These three curves (mirroring the first half or the second half and the average profiles) are shown in Fig. 2(c). The core edges, which correspond to the zero-deflection crossing points in the deflection curve, are also shown by dashed vertical lines. The actual value and error given from averaging the positions of the left and right edges of the optical core are also shown.

The RIP $n(r)$, where r is the distance from the preform axis, can be reconstructed by a transform operation expressed by the integration in Eq. (2) [6,17]:

$$n(r) = n_0\left[1 - \frac{1}{\pi}\int_r^a \tilde{\varphi}(x')(x'^2 - r^2)^{-1/2}\mathrm{d}x'\right]. \quad (2)$$

In Eq. (2), the modified deflection function $\tilde{\varphi}(r)$,

$$\tilde{\varphi} = \sin^{-1}\left[\frac{1}{n_0}\sin\varphi\right] \quad (3)$$

is used, which is corrected by taking into account Snell's law. n_0 is the refractive index of the surrounding index-matching oil. This is necessary for taking into account the ray deviation at the index-matching oil/air interface. The Δn profile, i.e., the difference between core and cladding refractive indices, calculated with this method is plotted in Fig. 2(d). In addition, the core edges are marked by dashed vertical lines for guidance.

The refractive-index profile appears mostly symmetric, with the core edges located symmetrically with respect to the core center within the error. Moreover, some micrometric features, which could be related to the multilayer structure of the sample, are VIS. The two dips present at the core edges are probably due to the residual presence of chlorine, which was used to fabricate the pure silica glass of the cladding. In Fig. 3, we compare measurements of the RIP performed in different positions along the preform length by our technique (red dashed lines) with those acquired with a commercial analyzer (PK 2600, Photon Kinetics), typically used in industrial refractive-index profilers of optical preforms.

The RIP calculated by our deflection measurements is in good agreement with that obtained by the commercial profiler. MCVD preforms are known to have RIPs that vary along their length in both height and width. The exact positions of the PK2600 profiles were not known to us at the time of experimentation. However, we found the same value of variability (± 0.0025) for the Δn along the preform length. The knowledge of the RIP is also useful in defining unambiguously the

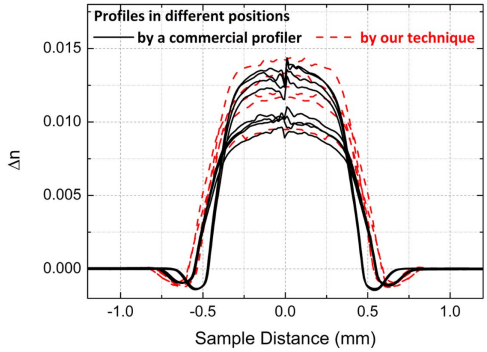

Fig. 3. Comparison between the RIP obtained by our technique and a set of curves derived from measurements on the same preform by a typical industrial refractive-index profiler (PK 2600).

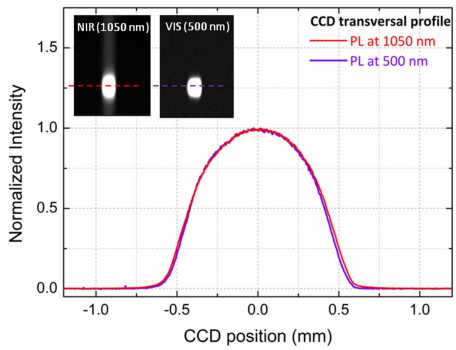

Fig. 4. Transversal profile extracted from the PL signal images acquired at 1050 (NIR) and 500 nm (VIS). The associated CCD images are shown as insets.

core edge positions and other refractive-index features which, in turn, helps in positioning the ADP accurately within the core of the preform. Without this knowledge, only the relative ADP position is determined. The ADP is obtained from the PL measurements. Figure 4 shows the profiles extracted from the CCD images (shown as insets) and related to the NIR and VIS PL signal acquired at 1050 and 500 nm, respectively. The signals at these wavelengths are signature of the PL of Yb^{3+}-single ions and Yb^{3+}-Yb^{3+} clusters, respectively. For an accurate comparison of the two profiles and correct determination of the Yb^{3+}-single ions and Yb^{3+}-Yb^{3+}-cluster distributions, we have corrected the detected data for the wavelength dependence of the magnification of the imaging system.

In order to confirm that the NIR and VIS PL are due to the de-excitation of Yb^{3+}-single ions and Yb^{3+}-Yb^{3+} clusters, respectively, we have plotted the exponential dependence of the emitted signal intensities (I_{PL}) on the pump excitation power (P_{EXC}), according to $I_{PL} \propto (P_{EXC})^m$, where m is the number of absorbed photons per up-converted emitted photon.

As shown in Fig. 5, we observed the expected linear dependence ($m \sim 1$) for the NIR emission of Yb^{3+}-ions at 1050 nm. The quadratic dependence ($m \sim 2$) of the VIS PL at 500 nm, on the other hand, confirms the two-photon process originating from a co-operative up-conversion in Yb^{3+}-Yb^{3+} clusters.

We applied the inverse Abel transformation to the PL profiles shown in Fig. 4. The spatial resolution of the current measurements, resulting from the high spatial frequency filtering, is

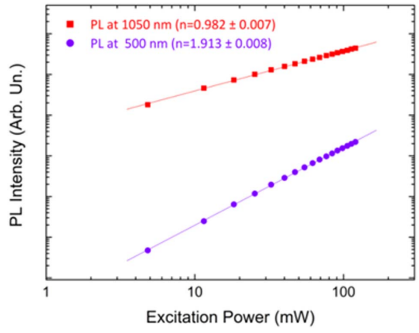

Fig. 5. Power laser excitation dependence of the PL intensity in (a) the NIR and (b) the VIS range.

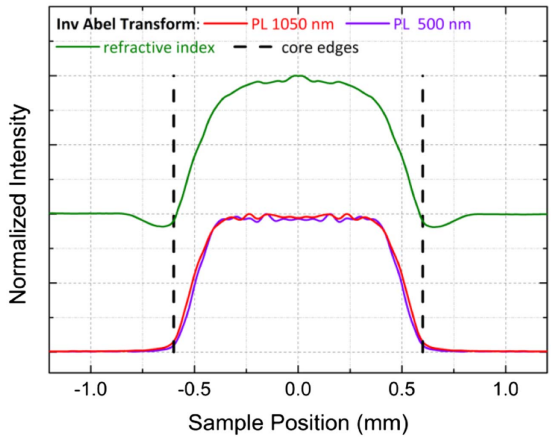

Fig. 6. Radial Yb^{3+}-emission profile, calculated by the application of an inverse Abel transform operation, related to the Yb^{3+}-ion and Yb^{3+}-Yb^{3+} cluster PL.

30 μm. Figure 6 shows the resulting ADPs for the Yb^{3+}-single ion and Yb^{3+}-Yb^{3+} clusters. It is shown that, in this case, the Yb^{3+} single ion and cluster distributions are very similar, following a substantially uniform distribution over the entire preform core. In the same figure, to facilitate a comparison, we also include the corresponding RIP [from Fig. 2(d)]. The small ripples, observed in the refractive-index and ADP profiles, are likely due to the multilayer structure of the optical core. Moreover, the uniform distribution of the Yb^{3+}-ions and ion clusters is mostly because of the Al codoping of the silica glass, which is known to increase the RE-ion solubility in the host silica matrix.

Finally, it is important to comment on the two additional approximations pertinent to this model. First, in obtaining the PL projections onto the CCD camera, we neglect the internal NIR absorption. This is a reasonable assumption, given that the NIR PL is centered at 1050 nm. Second, the deflection of the emitted photon as they traverse the preform is neglected, which is valid for samples with small refractive-index variations, as in the case reported in this Letter. Otherwise, a correction for that deflection should be considered [18].

In summary, we have developed a non-destructive technique to evaluate the Yb^{3+}-single ion and Yb^{3+}-Yb^{3+} cluster ADP distributions inside the core of optical fiber preforms. At the same time, the setup has been extended to include a means of measuring the corresponding RIP. The core RIP distribution was measured and used to define the precise location of the dopant within the core. The technique can be extended to characterize preforms with different dopants, such as erbium or thulium. The knowledge of the ADP distribution and its extent and other features within the core is extremely important in optimizing optical fibers for advanced applications requiring novel active fiber designs [19–21]. These advanced designs are critical for modal gain equalization in spatial-division-multiplexing telecom systems [22–24] and novel fibers for mitigating transverse modal instabilities in high-power fiber amplifiers [25,26].

Funding. Engineering and Physical Sciences Research Council (EPSRC) (EP/M020770/1).

Acknowledgment. The authors would like to thank Prof. J. K. Sahu for providing the preform and useful discussions. RAEng Research Chairs and Senior Research Fellowships scheme is also acknowledged. The data can be found in https://doi.org/10.5258/SOTON/D0540.

[†]The work was done when the author was affiliated with the ORC.

REFERENCES

1. A. E. Willner, R. L. Byer, C. J. Chang-Hasnain, S. R. Forrest, H. Kressel, H. Kogelnik, G. J. Tearney, C. H. Townes, and M. N. Zervas, Proc. IEEE **100**, 1604 (2012).
2. M. N. Zervas and C. A. Codemard, IEEE J. Sel. Top. Quantum Electron. **20**, 0904123 (2014).
3. S. Jetschke, S. Unger, A. Schwuchow, M. Leich, and J. Kirchhof, Opt. Express **16**, 15540 (2008).
4. A. D. Yablon and J. Jasapara, Proc. SPIE **8601**, 86011V (2013).
5. T. Okoshi, M. Nishimura, and M. Kosuge, Electron. Lett. **16**, 722 (1980).
6. I. Sasaki, D. N. Payne, and M. J. Adams, Electron. Lett. **16**, 219 (1980).
7. H. M. Presby and D. Marcuse, Appl. Opt. **18**, 671 (1979).
8. J. Kirchhof, S. Unger, A. Schwuchow, S. Jetschke, and B. Knappe, Proc. SPIE **5350**, 222 (2004).
9. M. Saha, A. Pal, and R. Sen, IEEE Photon. Technol. Lett. **26**, 58 (2014).
10. J. R. Marciante, R. G. Roides, V. V. Shkunov, and D. A. Rockwell, Opt. Lett. **35**, 1828 (2010).
11. Y. Yung, Q. Kang, V. A. J. M. Sleiffer, B. Inan, M. Kuschnerov, V. Veljanovski, B. Corbett, R. Winfield, Z. Li, P. S. Teh, A. Dhar, J. Sahu, F. Poletti, S. U. Alam, and D. J. Richardson, Opt. Express **21**, 10383 (2013).
12. M. Hino, T. Aono, M. Nakajima, and S. Yuta, Appl. Opt. **26**, 4742 (1987).
13. H. Uchiyama, M. Nakajima, and S. Yuta, Appl. Opt. **24**, 4111 (1985).
14. A. D. Yablon, Proc. SPIE **7914**, 79141N (2011).
15. R. Bracewell, *Fourier Analysis and Imaging* (Springer, 2003).
16. S. R. Deans, *The Transforms and Applications Handbook*, A. D. Poularikas, ed., 2nd ed. (CRC Press, 2000).
17. D. Marcuse, Appl. Opt. **18**, 9 (1979).
18. C. M. Vest, Appl. Opt. **14**, 1601 (1975).
19. J. Nilsson, R. Paschotta, J. E. Caplen, and D. C. Hanna, Opt. Lett. **22**, 1092 (1997).
20. R. S. Quimby, T. F. Morse, R. L. Shubochkin, and S. Ramachandran, IEEE J. Quantum Electron. **15**, 12 (2009).
21. T. Kokki, J. Koponen, M. Laurila, and C. Ye, Proc. SPIE **7580**, 758016 (2010).
22. Q. Kang, E.-L. Lim, Y. Jung, J. K. Sahu, F. Poletti, C. Baskiotis, S. Alam, and D. J. Richardson, Opt. Express **20**, 20835 (2012).
23. E. Ip, IEEE Photon. Technol. Lett. **24**, 1933 (2012).
24. D. Askarov and J. M. Kahn, IEEE Photon. Technol. Lett. **24**, 1945 (2012).
25. K. R. Hansen, T. T. Alkeskjold, J. Broeng, and J. Lægsgaard, Opt. Lett. **37**, 2382 (2012).
26. C. Robin, I. Dajani, and B. Pulford, Opt. Lett. **39**, 666 (2014).